

See discussions, stats, and author profiles for this publication at: <https://www.researchgate.net/publication/49764135>

Silica-Coated Gold Nanorods as Photoacoustic Signal Nanoamplifiers

ARTICLE *in* NANO LETTERS · FEBRUARY 2011

Impact Factor: 13.59 · DOI: 10.1021/nl1042006 · Source: PubMed

CITATIONS

156

READS

112

6 AUTHORS, INCLUDING:



[Yun-Sheng Chen](#)

Stanford University

43 PUBLICATIONS 688 CITATIONS

[SEE PROFILE](#)



[Seungsoo Kim](#)

Siemens

23 PUBLICATIONS 443 CITATIONS

[SEE PROFILE](#)



[Pieter Kruizinga](#)

Erasmus MC

15 PUBLICATIONS 310 CITATIONS

[SEE PROFILE](#)



[Kimberly Homan](#)

University of Texas at Austin

38 PUBLICATIONS 846 CITATIONS

[SEE PROFILE](#)

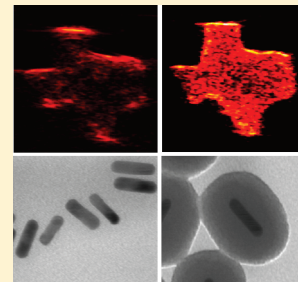
Silica-Coated Gold Nanorods as Photoacoustic Signal Nanoamplifiers

Yun-Sheng Chen,^{†,‡} Wolfgang Frey,[†] Seungsoo Kim,[†] Pieter Kruizinga,[†] Kimberly Homan,[†] and Stanislav Emelianov^{*,†,‡}

[†]Department of Biomedical Engineering and [‡]Department of Electrical and Computer Engineering, University of Texas at Austin, Austin, Texas 78712, United States

Supporting Information

ABSTRACT: Photoacoustic signal generation by metal nanoparticles relies on the efficient conversion of light to heat, its transfer to the environment, and the production of pressure transients. In this study we demonstrate that a dielectric shell has a strong influence on the amplitude of the generated photoacoustic signal and that silica-coated gold nanorods of the same optical density are capable of producing about 3-fold higher photoacoustic signals than nanorods without silica coating. Spectrophotometry measurements and finite difference time domain (FDTD) analysis of gold nanorods before and after silica coating showed only an insignificant change of the extinction and absorption cross sections, hence indicating that the enhancement is not attributable to changes in absorption cross section resulting from the silica coating. Several factors including the silica thickness, the gold/silica interface, and the surrounding solvent were varied to investigate their effect on the photoacoustic signal produced from silica-coated gold nanorods. The results suggest that the enhancement is caused by the reduction of the gold interfacial thermal resistance with the solvent due to the silica coating. The strong contrast enhancement in photoacoustic imaging, demonstrated using phantoms with silica-coated nanorods, shows that these hybrid particles acting as “photoacoustic nanoamplifiers” are high efficiency contrast agents for photoacoustic imaging or photoacoustic image-guided therapy.



KEYWORDS: Photoacoustic imaging, silica-coated gold nanorods, photoacoustic nanoamplifiers, medical and biological imaging, contrast agents

Photoacoustic imaging is a nonionizing and noninvasive imaging modality that combines the advantages of both optical and acoustic imaging.^{1–4} In photoacoustic imaging, the intensity modulated electromagnetic radiation, e.g., a beam of pulsed laser light, is directed at the imaging target. The light is absorbed and converted to an outgoing thermoacoustic wave that can be detected by an ultrasound transducer and used to reconstruct images.^{5–8} Since light is only used for heating and not for imaging, and acoustic waves are less scattered in optically turbid materials such as tissue, photoacoustic imaging can reach far deeper into turbid materials than purely optical imaging techniques.^{8,9} The contrast in photoacoustic imaging depends on the optical-to-acoustic conversion (optoacoustic) efficiency; i.e., how many incident photons can be absorbed and converted to heat, and how fast the generated heat can diffuse out from the target during thermoelastic expansion and wave generation. When a uniformly absorbing target is irradiated by pulsed light, the amplitude of the generated photoacoustic signal is proportional to the optical absorption and the thermal-acoustic properties of the absorbing medium. In contrast, in a heterogeneous medium such as a weakly absorbing solvent containing plasmonic nanoparticles, the amplitude of the photoacoustic signal depends strongly on the transfer of heat between the two materials.⁹ These heterogeneous systems are of particular interest for photoacoustic imaging because of their increased contrast, thus reducing image acquisition time and optical energy requirements to better accommodate *in vivo* imaging conditions.^{2,10–14}

Gold nanoparticles have been a common choice for contrast and therapeutic agents based on their superior optical properties,^{11–21} biocompatibility, and ease of bioconjugation with biomarkers to create nanosized contrast agents with molecular specificity.^{11–14,19,22–24} The conventional strategy of designing plasmonic photoacoustic contrast agents is usually to maximize the optical absorption cross section of nanoparticles by manipulating their size and shape and to choose the peak position and the relative amplitude of the absorption and scattering cross sections.^{25–27} Photoacoustic imaging has been demonstrated successfully using gold nanorods, nanocages, and nanoshells with high and tunable optical absorption cross sections.^{9,10,28–31} In this study, we introduce a new approach to significantly increase the contrast-to-noise ratio (CNR) of contrast-enhanced nanoparticle-augmented photoacoustic imaging by encapsulating gold nanorods within an optically nonabsorbing shell material, silica. The role of the silica shell in amplifying the photoacoustic signal highlights the importance of the heat transfer mechanism from the gold nanoparticle to the ambient signal-generating medium.

PEGylated and silica-coated gold nanorods prepared for this study are illustrated in Figure 1. The silica coating procedure followed our previously reported methods.^{32,33} Briefly, cetyltrimethylammonium

Received: July 25, 2010

Revised: January 11, 2011

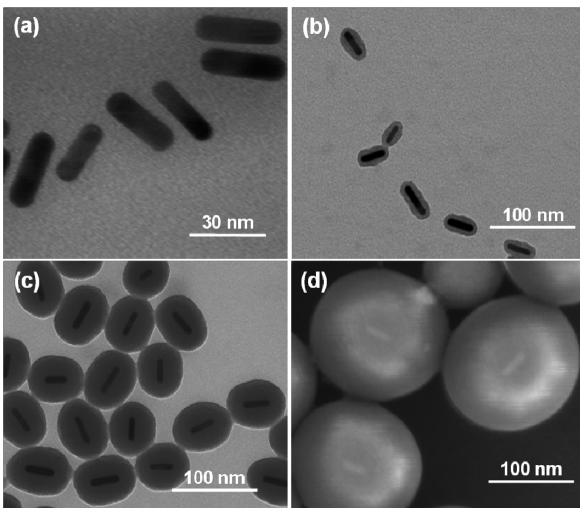


Figure 1. (a) TEM image of PEGylated gold nanorods. TEM images of gold–silica core–shell nanorods with (b) 6 ± 0.5 nm ($N = 100$) and (c) 20 ± 3.6 nm ($N = 100$) thickness of silica coating. (d) SEM image of gold–silica core–shell nanorods with 75 ± 5.0 nm ($N = 100$) thickness of silica coating (the silica shell is too thick for TEM).

bromide (CTAB) stabilized gold nanorods were first prepared with the seed-mediated growth method.^{34,35} Then CTAB was replaced by mPEG-thiol through ligand exchange, and then silica was grown onto the PEGylated gold nanorods via the modified Stöber method using tetraethyl orthosilicate (TEOS).^{36,37} As seen in Figure 1, there is conformal and isotropic silica coating of the gold nanorods with controllable silica thickness.

We have previously shown the usefulness of silica-coated nanorods for photoacoustic imaging and photothermal therapy due to their stability under high-fluence laser pulses.^{32,33} In order to investigate the effect of the silica coating on the photoacoustic signal response, we performed a study using poly(vinyl alcohol) (PVA) tissue-mimicking phantoms containing inclusions made out of gelatin mixed with gold nanorods. The four types of gold nanorods presented in Figure 1 were used to prepare the inclusions. To ensure the same level of absorption between inclusions, the extinction of each gold nanorod solution was adjusted to 3 (in 1 cm optical path), which corresponds to about 3.8×10^{12} (particles/mL), as determined by ultraviolet–visible (UV–vis) spectroscopy. The nanorods were mixed with equal amounts of a 10 wt % gelatin aqueous solution. The experimental setup for the photoacoustic imaging is shown in Figure S1 of the Supporting Information. A laser beam (5 ns pulse duration, 10 Hz repetition rate) was generated by a tunable OPO laser system (Premiscan, GWU, Inc.) pumped by a pulsed Nd:YAG laser (Quanta-Ray, Spectra Physics, Inc.). The wavelength of the light in this and in all other experiments was matched to the peak absorption of each type of gold nanorods (786, 790, 802, and 806 nm for 0, 6, 20, and 75 nm silica shell thickness, respectively). The laser beam was expanded to fully illuminate the entire inclusion. An ultrasound microimaging system (Vevo 2100, Visualsonics, Inc.) equipped with an array ultrasound transducer (MS550, Visualsonics, Inc.) operating at 40 MHz center frequency was used to acquire the cross-sectional B-scan and photoacoustic images of the phantom with inclusions. The position of the ultrasound transducer was first adjusted so that the focus of the transducer was located at the center of the inclusion, and the distance between the transducer and the inclusion was then kept constant

for all inclusions. The average fluence of the laser beam was maintained at 6 mJ/cm^2 —a fluence that is below the damage threshold for PEGylated gold nanorods, to allow for a quantitative comparison between the photoacoustic signals and images of the inclusions.³² All experiments were performed at room temperature.

Figure 2 shows a comparison of ultrasound, photoacoustic, and the spatially coregistered combined ultrasonic and photoacoustic images of phantoms with inclusions containing PEGylated gold nanorods, and gold–silica core shell nanorods with silica shells of 6, 20, and 75 nm thickness, respectively. Inclusion with PEGylated gold nanorods produced a much weaker photoacoustic signal than inclusions with silica-coated nanorods—even the nanorods with 6 nm silica shell had noticeable photoacoustic signal enhancement. As the thickness of the silica shell increases from 6 to 20 nm, the photoacoustic signal increases and, consequently, the photoacoustic image appears brighter. The signal enhancement is slightly reduced for the nanorods with a 75 nm silica shell.

The quantitative analysis of the photoacoustic signal enhancement is presented in Figure 3 (for details of the analysis see the Supporting Information). The average amplitude of the normalized photoacoustic signal measured from the inclusions containing PEGylated gold nanorods, 6, 20, and 75 nm silica coated gold nanorods, is 14.00 ± 5.40 , 28.00 ± 11.00 , 53.00 ± 15.00 , and 32.00 ± 12.00 , respectively (Figure 3a). The photoacoustic signal from the gold nanorods with 20 nm silica shell is about 3.8 times higher compared to PEGylated nanorods while the amplitude of the photoacoustic signal from the background (i.e., noise) remains relatively the same for each phantom. Correspondingly, the contrast-to-noise ratio (CNR) of the photoacoustic images of inclusions with PEGylated, 6, 20, and 75 nm silica-coated gold nanorods were 9.0, 10.1, 13.5, and 10.7 dB, respectively (Figure 3b). Again, the 20 nm silica-coated gold nanorods exhibit a more than 2.8 times (4.5 dB) enhancement of contrast and CNR compared to traditional PEGylated gold nanorods.

Since the photoacoustic amplitude is proportional to the optical absorption, one would expect that the strong increase in the photoacoustic signal is a result of a changed absorption cross section of the gold nanorods due to the change of the immediate environment (i.e., the silica shell acting as a layer between the gold surface of the nanorod and the surrounding material such as water). To show that this is not the case, a series of UV–vis spectra of gold nanorods before and after silica coating was collected. To ensure that the concentration of gold nanorods was constant, 100 μL of the nanorod solution was taken at the beginning and at different time points during the silica shell growth process from the growth solution. Figure 4a shows the measured extinction spectra of gold nanorods recorded at the start of the silica coating process and as the silica coating reached 75 nm thickness. The synthesized gold nanorods, as illustrated in Figure 1, have an aspect ratio of 3.9 ± 0.38 resulting in a longitudinal plasmon resonance at 786 nm. After coating the nanorods with silica shells of 6, 20, and 75 nm thickness, the longitudinal peak red shifts to 790, 802, and 806 nm correspondingly. The amplitude of extinction after 6 nm silica coating drops 3% and then gradually increases back to the same amplitude as for the PEGylated gold nanorods due to the increasing contribution of light scattering. The shape of the peak is preserved suggesting that the silica coating did not alter the shape or cause noticeable aggregation of the nanorods. This was also confirmed by an analysis of

113
114
115
116
117
118
119 F2
120
121
122
123
124
125
126
127
128
129
130
131
132
133 F3
134
135
136
137
138
139
140
141
142
143
144
145
146
147
148
149
150
151
152
153
154
155
156
157
158
159
160
161 F4
162
163
164
165
166
167
168
169
170
171
172
173
174

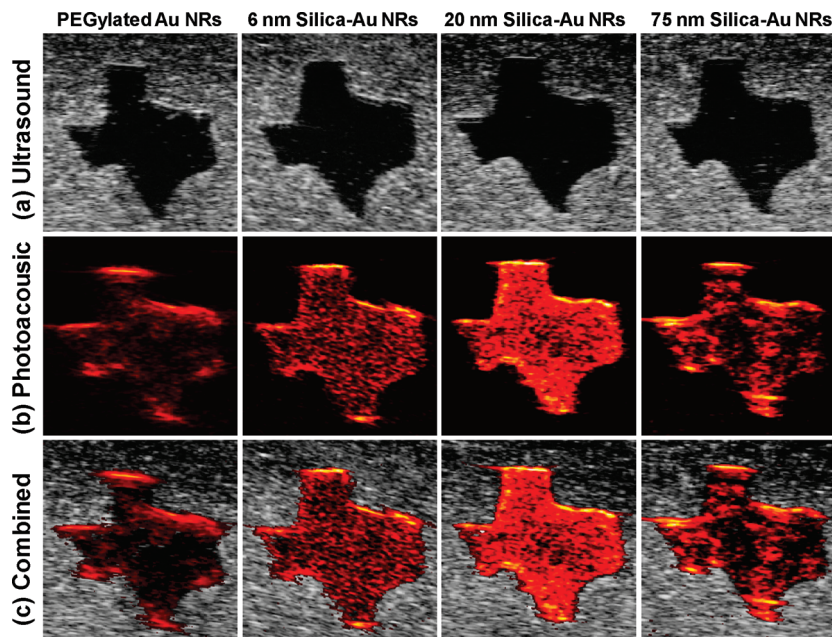


Figure 2. (a) Ultrasound, (b) photoacoustic, and (c) combined ultrasound and photoacoustic images (top to bottom) of inclusions containing (I) PEGylated gold nanorods and gold–silica core–shell nanorods with (II) 6 nm silica coating, (III) 20 nm silica coating, and (IV) 75 nm silica coating (left to right). Each image covers a 6 mm by 6 mm field of view.

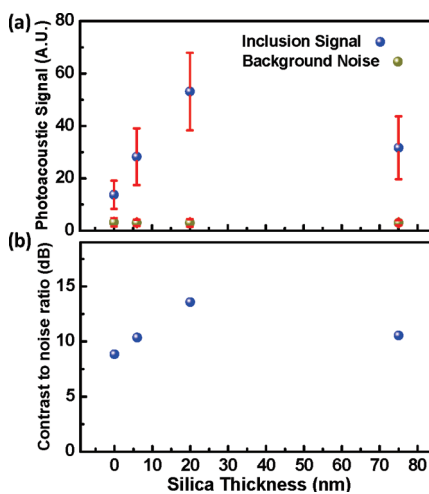


Figure 3. (a) Amplitude of the photoacoustic signal from the background (green dots) and inclusions (blue dots) containing gold nanorods with varying thickness of the silica coating. The error bars show ± 1 standard error. (b) Contrast-to-noise ratios (CNRs) of the photoacoustic images of the inclusions containing gold nanorods with varying thickness of the silica coating.

the TEM images. Most importantly, the amplitude of the extinction at the resonance is unchanged.

Finite difference time domain (FDTD) simulations (FDTD Solutions, Lumerical, Inc.) confirmed that the silica coating insignificantly alters the amplitude of the extinction cross section of gold nanorods ($\sim 1.8\%$) and that the amplitude of the absorption cross section, which is responsible for the photoacoustic signal, is also practically unchanged ($\sim 2\%$). Figure 4b presents the calculated absorption and scattering cross sections for gold nanorods before and after 10, 20, and 60 nm silica coating. The scattering cross section, which is nearly 2 orders of magnitude lower

than the absorption cross section and is shown in an enlarged scale in Figure 4b for clarity. The peaks are less broad compared to measured spectra—this is due to small variations in the aspect ratio of the synthesized nanorods. The insignificant scattering by nanorods with and without silica shell indicates that a small number of spheroid particles in the synthesis solution leads to the increased background seen in the experiment (Figure 4a). However, without background signal, the area under the measured peak decreases only slightly with silica thickness, which most likely indicates some decrease in the yield of the synthesis. The peak is shifted further to the red compared to the experiment because, as discussed previously,³² the silica shell is less dense than the fused silica used in the simulation. Because the absorption cross section changes insignificantly and the laser wavelength in each photoacoustic experiment was adjusted to the peak absorption of each sample, we can exclude a change in the absorption cross section as the cause of the photoacoustic signal amplification.

After excluding a change in the absorptive properties of the gold nanorod due to silica coating as the reason for the increase in the photoacoustic response, changes in the thermal transport from the gold nanorod to the signal generating fluid environment were investigated. The amplitude of the photoacoustic signal for a small source at nanosecond time scales is related to the temporal temperature gradient generated in the surrounding medium by the heat diffusing from the nanorod.^{5–7,38} Assuming a diffusive heat transport process, adding a shell of any material with finite heat conductance and capacity will only broaden a heat pulse and deteriorate the photoacoustic signal. However, the same signal deterioration results from a high interfacial thermal resistance between the heat pulse exiting the gold nanorod and entering the ambient medium. This high resistance would lead to a much higher nanoparticle temperature, and a slower heat release into the adjacent medium. Conversely, a low interfacial thermal resistance leads to fast heat transfer and a temperature profile that much more closely resembles the profile of the laser

186
187
188
189
190
191
192
193
194
195
196
197
198
199
200
201
202
203
204
205
206
207
208
209
210
211
212
213
214
215
216
217
218
219
220

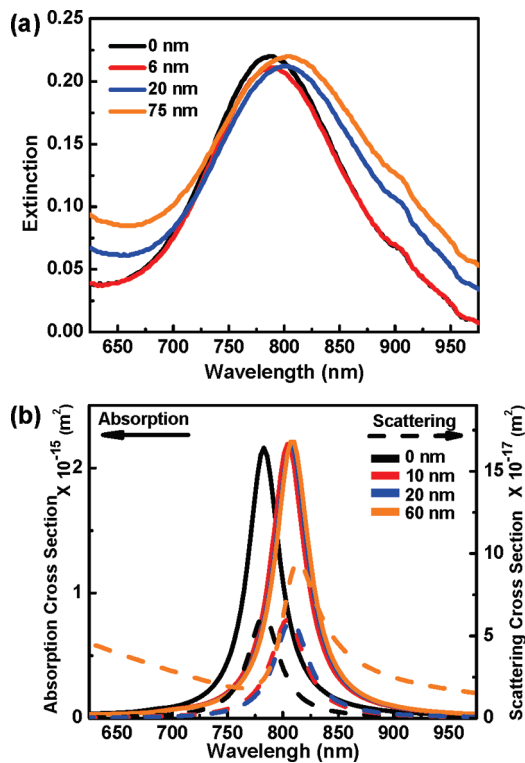


Figure 4. (a) Extinction spectra of a gold nanorod solution before and after 6, 20, and 75 nm silica coating. (b) FDTD simulated absorption (solid curve) and scattering (dashed curve) cross-section spectra of gold nanorods before (black line) and after coating with 10 nm (red line), 20 nm (blue line), and 60 nm (orange line) silica. The simulations were performed using the refractive index of fused silica. Note that scattering is nearly 2 orders of magnitude lower than the absorption.

pulse and leads to a stronger photoacoustic signal. The interfacial thermal resistance originates from the scattering or reflection of phonons at the gold dielectric interface and causes a discontinuity of the thermal profile at the interface of the form $\Delta T = RQ$, where Q is the heat flux through the interface and R is the interfacial resistance.^{39–41}

In the case of PEGylated gold nanorods, the interfaces of gold to surface layer and surface layer to water play a role. In the case of silica-coated gold nanorods, the interfaces of gold to surface layer, surface layer to silica, and silica to water exist. Studies of the heat conductance from flat gold surfaces coated with alkylthiols of varying length showed that the heat transfer process was linear with chain length but that it was dominated by the Au–S interface resistance.⁴² The interfacial thermal conductance, which is the inverse of the interfacial thermal resistance, for this interface was found to be 200–250 MW m⁻² K⁻¹, very similar to Au–Pd nanoparticles stabilized with monohydroxy(1-mercaptopoundec-11-yl)tetraethylene glycol (EG-4) and CTAB,⁴³ and gold nanorods stabilized with CTAB.⁴⁴ This value is about two times the interfacial thermal conductance for citrate stabilized gold nanoparticles in water,^{45,46} while the calculated value for a pure gold–water interface of 170 MW m⁻² K⁻¹ lies in between.⁴⁷ However, these values depend strongly on the solvent; the interfacial conductivity for the same thiol coated Au–Pd nanoparticles in toluene is an order of magnitude lower.^{43,48} The thermal conductance for the interface of a thin solution-grown silica layer to gold is not known. Some reports place the conductance relatively low for solid–solid interfaces, with the Au–dielectric

conductance at 40 MW m⁻² K⁻¹ independent of the dielectric,⁴⁹ and Au–glass conductance at 100 MW m⁻² K⁻¹ for glass with a silica content of 53%,⁵⁰ and 60 MW m⁻² K⁻¹ for gold on thermally grown thin silica films.⁵¹ However, the structure of the silica and details of the interface play an important role⁵¹ and interfacial heat conductance in excess of 220 MW m⁻² K⁻¹ have been measured for more grainy gold films,⁵² which is in better agreement with what our results suggest. In contrast, the silica to water interface has a very high thermal conductance in excess of 1000 MW m⁻² K⁻¹ as determined by molecular dynamics.^{53,54} The large spread of interfacial thermal conductances between different interfaces highlights the importance of the molecular interactions, such as hydrogen bonding between the hydroxyl head groups of silica and water. Accordingly, terminal functionality of thiols and silanes has been shown to strongly influence the effective interfacial conductance for gold and silica to water with hydrophobic groups showing \sim 50 MW m⁻² K⁻¹ for gold⁵⁴ and \sim 200 MW m⁻² K⁻¹ for silica.⁵³

While it is clear that introducing a silica–water surface will increase the interfacial conductance, the gold to silica surface may have a relatively high thermal interface resistance. However, coating gold nanoparticles with a shell has been found to increase the heat conductance from the gold core to the ambient medium. Ge and co-workers coated gold spheres with a polymeric shell and found the heat conductance to be faster than expected from bulk materials properties and interfacial conductance if a small amount of a cosolvent was added to the aqueous medium.⁴⁶ Very much in agreement with our results, Hu et al. reported faster heat dissipation from silica-coated gold nanospheres than from bare gold nanoparticles in water.⁵⁵ We therefore expected that the photoacoustic signal enhancement must come from an increased thermal transfer through the gold interface induced by changing the interface from gold–(PEG)–water to gold–(PEG)–silica–water and that the signal increase should be sensitive to an exchange of the environment from water to oil.

To experimentally demonstrate the influence of the interfacial heat conductance on the photoacoustic response, two sets of experiments were conducted to separately investigate the two interfaces of silica-coated gold nanorods. The first set of experiments was focused on studying the thermal conductance at the gold/silica interface in aqueous solution. Three types of gold nanorods were prepared: CTAB stabilized gold nanorods, gold nanorods coated with mPEG-thiol (MW 2000 Da), and CTAB stabilized gold nanorods coated with an electrostatically stabilized multilayer created by sequential layer-by-layer deposition of poly(styrenesulfonate) (PSS, MW 14900 Da), poly(allylamine hydrochloride) (PAH, MW 15000 Da), and poly(vinylpyrrolidone) (PVP, MW 10000 Da) following the procedure reported by Pastoriza-Santos et al.⁵⁶ These three types of gold nanorods have all been successfully used for subsequent silica coating^{32,33,56,57} but have an increasing thickness of the organic passive layer. The thicknesses of CTAB, PEG, and multilayer polyelectrolyte are about 4–5,⁵⁸ 6–7,^{59,60} and 7–8 nm,⁵⁹ respectively. The concentrations were adjusted so that the extinctions of each gold nanorod type were the same. The amplitudes of the photoacoustic signal from 60 pulses were recorded, and the average and the standard deviation are reported for each nanorod type. (The same experiment was performed twice with two different batches of gold nanorods; the absolute photoacoustic amplitudes differ from those in Figure 3 because of different concentrations and experimental setup. See Supporting Information (Figure S5).) Before silica coating, CTAB and PEGylated gold nanorods show similar

249
250
251
252
253
254
255
256
257
258
259
260
261
262
263
264
265
266
267
268
269
270
271
272
273
274
275
276
277
278
279
280
281
282
283
284
285
286
287
288
289
290
291
292
293
294
295
296
297
298
299
300
301
302
303
304
305
306
307
308
309 F5
310

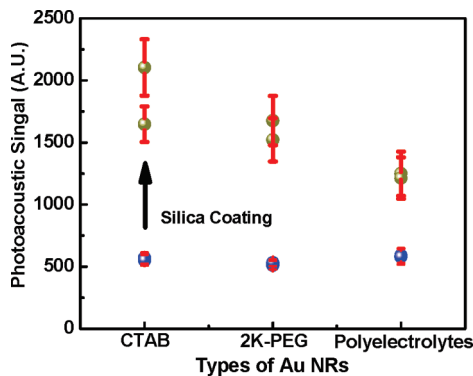


Figure 5. Average amplitudes of the photoacoustic signal from three types of gold nanorods before and after silica coating. The error bars represent ± 1 standard deviation of the photoacoustic signal measured using 60 laser pulses of low (4 mJ/cm^2) fluence.

photoacoustic signal amplitudes, while a slightly higher signal was found for the polyelectrolyte-coated gold nanorods. After the nanorods were coated with 20 nm of silica, all three types of nanorods show significantly elevated photoacoustic signals, but to different levels. The silica-coated CTAB gold nanorods show the largest enhancement and the silica-coated polyelectrolyte-multilayer gold nanorods show the lowest signal enhancement. These different nanorods represent different interfaces of gold with silica and have been shown to modulate the interfacial heat conductance.⁵⁹ Since the CTAB layer is extremely thin, and the CTAB is almost totally exchanged with silica during the coating process;⁵⁷ these nanorods come closest to the exact interface between gold and silica. However, since both the PEG layer and the polyelectrolyte multilayer have finite thickness, the results show a decreasing enhancement with increasing layer thickness. It is unclear, however, whether this thickness dependence represents a direct correlation or whether factors such as interpenetration of silica into the organic layer or surface coverage play a role. Such influences are suggested by the CTAB nanorod experiments, which show a large variation between batches and are known to be the least controlled way to generate the silica coating.

In a second set of experiments, the interface between silica and the surrounding media was investigated (experimental details can be found in the Supporting Information (Figure S4)). Three different solvents, the silica growth solution (a water/IPA mixture which contains 26 vol % of water), water, and silicone oil were utilized to immerse PEGylated gold nanorods and silica-coated gold nanorods with various coating thickness. The absolute value of the photoacoustic signal in oil, IPA, and water is generally different due to the differences in Grüneisen parameter and experimental setups, but this is of no importance to the arguments made here. Figure 6 shows an increasing photoacoustic signal with increasing silica thickness from 0 to 20 nm in polar solvent, while in oil, the opposite trend, a decrease in photoacoustic signal with increasing silica thickness up to 20 nm is observed. PEGylated gold nanorods have a less hydrophilic surface due to the methyl terminal groups than silica, and when immersed in oil, a higher interfacial thermal conductance could be expected compared to water. On the other hand, the hydroxyl groups of the silica surface are able to form hydrogen bonds with water, and have been shown to have a high interfacial thermal conductance.

The equal photoacoustic signal from PEG- and CTAB-coated nanorods is in agreement with the thermal behavior seen for

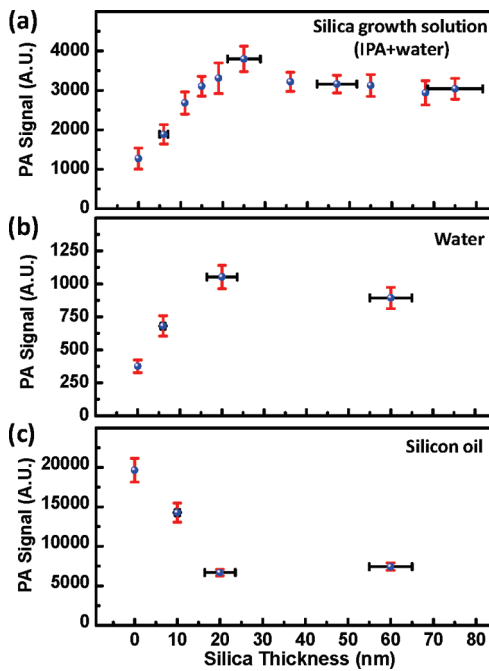


Figure 6. Photoacoustic signal amplitude of gold nanorods with varying thickness of the silica coating in (a) silica growth solution (IPA containing 26 vol % water), (b) water, and (c) silicone oil. In a polar environment the signal is amplified and shows a maximum at ~ 20 nm shell thickness, while in a nonpolar environment the signal monotonically decreases. The vertical error bars represent ± 1 standard deviation of the photoacoustic signal measured using 60 laser pulses of low (4 mJ/cm^2) fluence. The horizontal error bars represent ± 1 standard deviation of the silica thickness measured by TEM.

Au–Pd nanoshells,⁴³ although our PEG is larger and methyl rather than hydroxyl-terminated. The strongly increased signal due to silica coating in water contradicts a direct coupling of the silica with the gold surface as this should have a decreased interfacial conductance.⁵⁰ The results shown in Figure 2 and Figure 6b demonstrate, however, that the parameters that characterize each interface have a strong influence on the thermal conductance and, therefore, on the photoacoustic signal. Whether the signal increase by a factor of 3 can be explained fully by an improved thermal interfacial conductance or whether increased thermal diffusion along water channels in the silica shell may play a role and whether the improved conductance leads to nonlinear effects in the photoacoustic signal generation due to the temperature dependence of the thermal expansion coefficient of water⁶ is currently under investigation.

It is interesting that the photoacoustic response change due to the introduction of a silica shell is not a simple step but a biphasic profile in the case of the polar solvent and a continuous decrease in the case of oil. The maximum at around 20 nm silica shell thickness in polar solvents is significantly higher than the signal at thicker shells ($p < 10^{-4}$, pairwise t test). We attribute the gradual increase to imperfections in the coating for thin silica layers below ~ 20 nm. For thicker silica layers we expect that the thermal pulse profile exhibits some broadening due to the finite thermal conduction of silica, even though silica has a good thermal conduction. The signal enhancement effect due to an increase in interfacial conductance is partially canceled by this signal broadening above a thickness of 20 nm in polar solvent. Additionally, the increased scattering of the larger silica-coated nanoparticles

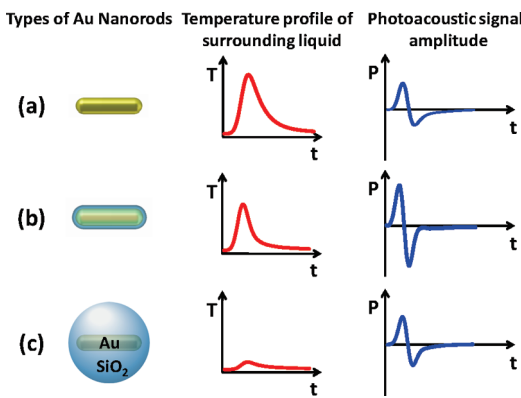


Figure 7. Schematic summary of the proposed thermal transport processes from the nanoparticle to the environment and the resulting temporal profiles of the temperature (T) near the surface and the amplitude of the photoacoustic signal (P) far from the surface of the nanoparticle. (a) A bare nanoparticle with high interfacial resistance leads to a broadened temperature profile and a smaller amplitude of the photoacoustic pressure signal. (b) Introducing a silica shell leads to a minimal interfacial resistance between gold (Au) and SiO_2 and SiO_2 and water. The resulting sharper temperature profile, and because the temperature profile is at a larger distance, the photoacoustic signal is increased. (c) A thick shell leads to a broadened temperature peak and again a decrease in the photoacoustic signal, although it may still be higher than that for the bare nanoparticle.

could lead to a reduced local fluence and so also contribute to the reduced PA signal. On the other hand, in silicone oil, the interfacial conductance of the silica/oil interface is lower than that of the PEG/oil interface, and together with the heat pulse broadening and the scattering both contribute to the signal reduction.

Figure 7 shows a schematic summary of the proposed mechanism for the photoacoustic signal enhancement from silica-coated nanoparticles, emphasizing the importance of the heat transfer to the water. While nanoparticles with no shell have a slower heat transfer resulting in a broader heat peak due to their interfacial properties, adding a silica shell reduces the interfacial resistance and leads to a sharper peak even though its amplitude may be reduced due to the heat capacity of silica. At very large thickness the influence of the bulk silica is stronger leading to a further reduced and somewhat broader temperature peak. Because the pressure is roughly proportional to the slope, but includes also a geometric term that grows with the size of the heated liquid, the slightly sharper pulse of a larger particle leads to a higher photoacoustic signal. Additionally, changes in the frequency spectrum of the signals may be possible, which we have not investigated here.

In conclusion, this study has shown that silica-coated gold nanorods can amplify the photoacoustic response without altering the optical absorption of nanoparticles other than shifting it slightly to the red. The signal enhancement of silica-coated gold nanorods in water depends on the silica thickness in a biphasic way. The enhancement could be attributed to changes in the interfacial heat conduction from gold to water due to the silica. The biphasic behavior reflects the balance between changing the interfacial conduction and the profile flattening due to a finite bulk heat conductivity and capacity by adding a dielectric shell. Silica coating of gold nanoparticles appears to be a simple way to increase their usefulness as contrast agents for photoacoustic imaging.

■ ASSOCIATED CONTENT

S Supporting Information. Details of experiments and additional supplementary figures. This material is available free of charge via the Internet at <http://pubs.acs.org>

■ AUTHOR INFORMATION

Corresponding Author

*E-mail: emelian@mail.utexas.edu.

■ ACKNOWLEDGMENT

Partial support from the National Institutes of Health under Grants CA149740 and EB008101 is acknowledged. We thank the National Science Foundation (Grant No. 0821312) for funding the Hitachi S-5500 SEM/STEM used in this work.

■ REFERENCES

- (1) Emelianov, S. Y.; Aglyamov, S. R.; Shah, J.; Sethuraman, S.; Scott, W. G.; Schmitt, R.; Motamedi, M.; Karpouli, A.; Oraevsky, A. *Proc. SPIE* **2004**, *5320*, 101–112.
- (2) Emelianov, S. Y.; Li, P. C.; O'Donnell, M. *Phys. Today* **2009**, *62* (5), 34–39.
- (3) Wang, X.; Pang, Y.; Ku, G.; Xie, X.; Stoica, G.; Wang, L. V. *Nat. Biotechnol.* **2003**, *21* (7), 803–806.
- (4) Zhang, H. F.; Maslov, K.; Stoica, G.; Wang, L. H. V. *Nat. Biotechnol.* **2006**, *24* (7), 848–851.
- (5) Diebold, G. J.; Beveridge, A. C.; Hamilton, T. J. *J. Acoust. Soc. Am.* **2002**, *112* (5), 1780–1786.
- (6) Calasso, I. G.; Craig, W.; Diebold, G. J. *Phys. Rev. Lett.* **2001**, *86* (16), 3550–3553.
- (7) Cox, B. T.; Beard, P. C. *J. Acoust. Soc. Am.* **2005**, *117* (6), 3616–3627.
- (8) Xu, M. H.; Wang, L. H. V. *Rev. Sci. Instrum.* **2006**, *77* (4), 22.
- (9) Oraevsky, A. A.; Karabutov, A. A.; Savateeva, E. V. *Proc. SPIE* **2001**, *4434*, 60–69.
- (10) Agarwal, A.; Huang, S. W.; O'Donnell, M.; Day, K. C.; Day, M.; Kotov, N.; Ashkenazi, S. *J. Appl. Phys.* **2007**, *102* (6), 064701.
- (11) Kim, J. W.; Galanze, E. I.; Shashkov, E. V.; Moon, H. M.; Zharov, V. P. *Nat. Nanotechnol.* **2009**, *4* (10), 688–694.
- (12) Li, P. C.; Wang, C. R. C.; Shieh, D. B.; Wei, C. W.; Liao, C. K.; Poe, C.; Jhan, S.; Ding, A. A.; Wu, Y. N. *Opt. Express* **2008**, *16* (23), 18605–18615.
- (13) Mallidi, S.; Larson, T.; Aaron, J.; Sokolov, K.; Emelianov, S. *Opt. Express* **2007**, *15* (11), 6583–6588.
- (14) Chen, J. Y.; Wang, D. L.; Xi, J. F.; Au, L.; Siekkinen, A.; Warsen, A.; Li, Z. Y.; Zhang, H.; Xia, Y. N.; Li, X. D. *Nano Lett.* **2007**, *7* (5), 1318–1322.
- (15) West, J. L.; Halas, N. J. *Annu. Rev. Biomed. Eng.* **2003**, *5*, 285–292.
- (16) Huang, X. H.; El-Sayed, I. H.; Qian, W.; El-Sayed, M. A. *J. Am. Chem. Soc.* **2006**, *128* (6), 2115–2120.
- (17) Huang, X. H.; Jain, P. K.; El-Sayed, I. H.; El-Sayed, M. A. *Lasers Med. Sci.* **2008**, *23* (3), 217–228.
- (18) Mallidi, S.; Larson, T.; Tam, J.; Joshi, P. P.; Karpouli, A.; Sokolov, K.; Emelianov, S. *Nano Lett.* **2009**, *9* (8), 2825–2831.
- (19) Jain, P. K.; El-Sayed, I. H.; El-Sayed, M. A. *Nano Today* **2007**, *2* (1), 18–29.
- (20) Johnson, P. B.; Christy, R. W. *Phys. Rev. B* **1972**, *6* (12), 4370–4379.
- (21) Rozanova, N.; Zhang, J. Z. *Sci. China, Ser. B: Chem.* **2009**, *52* (10), 1559–1575.
- (22) Kumar, S.; Harrison, N.; Richards-Kortum, R.; Sokolov, K. *Nano Lett.* **2007**, *7* (5), 1338–1343.
- (23) Loo, C.; Lowery, A.; Halas, N.; West, J.; Drezek, R. *Nano Lett.* **2005**, *5* (4), 709–711.

- 479 (24) Kumar, S.; Aaron, J.; Sokolov, K. *Nat. Protoc.* **2008**, 3 (2), 314–
480 320.
481 (25) Kelly, K. L.; Coronado, E.; Zhao, L. L.; Schatz, G. C. *J. Phys.*
482 *Chem. B* **2003**, 107 (3), 668–677.
483 (26) Lee, K.; El-Sayed, M. A. *J. Phys. Chem. B* **2006**, 110 (39),
484 19220–19225.
485 (27) Jain, P. K.; Lee, K. S.; El-Sayed, I. H.; El-Sayed, M. A. *J. Phys.*
486 *Chem. B* **2006**, 110 (14), 7238–7248.
487 (28) Skrabalak, S. E.; Chen, J. Y.; Sun, Y. G.; Lu, X. M.; Au, L.;
488 Cobley, C. M.; Xia, Y. N. *Acc. Chem. Res.* **2008**, 41 (12), 1587–1595.
489 (29) Yang, X. M.; Skrabalak, S. E.; Li, Z. Y.; Xia, Y. N.; Wang, L. H. V.
490 *Nano Lett.* **2007**, 7 (12), 3798–3802.
491 (30) Li, M. L.; Wang, J. C.; Schwartz, J. A.; Gill-Sharp, K. L.; Stoica,
492 G.; Wang, L. H. V. *J. Biomed. Opt.* **2009**, 14 (1), No. 010507.
493 (31) Kim, C.; Cho, E. C.; Chen, J.; Song, K. H.; Au, L.; Favazza, C.;
494 Zhang, Q.; Cobley, C. M.; Gao, F.; Xia, Y.; Wang, L. V. *ACS Nano* **2010**,
495 4 (8), 4559–4564.
496 (32) Chen, Y. S.; Frey, W.; Kim, S.; Homan, K.; Kruizinga, P.;
497 Sokolov, K.; Emelianov, S. *Opt. Express* **2010**, 18 (9), 8867–8877.
498 (33) Chen, Y. S.; Kruizinga, P.; Joshua, P.; Kim, S.; Homan, K.;
499 Sokolov, K.; Frey, W.; Emelianov, S. *Proc. SPIE* **2010**, 7564, 75641Q–
500 75641Q8.
501 (34) Jana, N. R.; Gearheart, L.; Murphy, C. J. *Adv. Mater.* **2001**, 13
502 (18), 1389–1393.
503 (35) Nikoobakht, B.; El-Sayed, M. A. *Chem. Mater.* **2003**, 15 (10),
504 1957–1962.
505 (36) Lu, Y.; Yin, Y. D.; Mayers, B. T.; Xia, Y. N. *Nano Lett.* **2002**, 2
506 (3), 183–186.
507 (37) Stober, W.; Fink, A.; Bohn, E. *J. Colloid Interface Sci.* **1968**, 26
508 (1), 62–69.
509 (38) Frez, C.; Diebold, G. *J. Eur. Phys. J. Spec. Top.* **2008**, 153, 307–
510 311.
511 (39) Swartz, E. T.; Pohl, R. O. *Rev. Mod. Phys.* **1989**, 61 (3), 605–
512 668.
513 (40) Murad, S.; Puri, I. K. *Chem. Phys. Lett.* **2008**, 467 (1–3), 110–
514 113.
515 (41) Cahill, D. G.; Ford, W. K.; Goodson, K. E.; Mahan, G. D.;
516 Majumdar, A.; Maris, H. J.; Merlin, R.; Phillpot, S. R. *J. Appl. Phys.* **2003**,
517 93 (2), 793–818.
518 (42) Wang, Z. H.; Carter, J. A.; Lagutchev, A.; Koh, Y. K.; Seong,
519 N. H.; Cahill, D. G.; Dlott, D. D. *Science* **2007**, 317 (5839), 787–790.
520 (43) Ge, Z. B.; Cahill, D. G.; Braun, P. V. *J. Phys. Chem. B* **2004**, 108
521 (49), 18870–18875.
522 (44) Schmidt, A. J.; Alper, J. D.; Chiesa, M.; Chen, G.; Das, S. K.;
523 Hamad-Schifferli, K. *J. Phys. Chem. C* **2008**, 112 (35), 13320–13323.
524 (45) Plech, A.; Kotaidis, V.; Gresillon, S.; Dahmen, C.; von Plessen,
525 G. *Phys. Rev. B* **2004**, 70 (19), No. 195423.
526 (46) Ge, Z. B.; Kang, Y. J.; Taton, T. A.; Braun, P. V.; Cahill, D. G.
527 *Nano Lett.* **2005**, 5 (3), 531–535.
528 (47) Merabia, S.; Shenogin, S.; Joly, L.; Kebinski, P.; Barrat, J. L.
529 *Proc. Natl. Acad. Sci. U.S.A.* **2009**, 106 (36), 15113–15118.
530 (48) Wilson, O. M.; Hu, X. Y.; Cahill, D. G.; Braun, P. V. *Phys. Rev. B*
531 **2002**, 66 (22), No. 224301.
532 (49) Stoner, R. J.; Maris, H. J. *Phys. Rev. B* **1993**, 48 (22), 16373–
533 16387.
534 (50) Juve, V.; Scardamaglia, M.; Maioli, P.; Crut, A.; Merabia, S.;
535 Joly, L.; Del Fatti, N.; Vallee, F. *Phys. Rev. B* **2009**, 80 (19), No. 195406.
536 (51) Burzo, M. G.; Komarov, P. L.; Raad, P. E. *IEEE Trans. Compon.*
537 *Packag. Technol.* **2003**, 26 (1), 80–88.
538 (52) Kato, R.; Hatta, I. *Int. J. Thermophys.* **2008**, 29 (6), 2062–2071.
539 (53) Schoen, P. A. E.; Michel, B.; Curioni, A.; Poulikakos, D. *Chem.*
540 *Phys. Lett.* **2009**, 476 (4–6), 271–276.
541 (54) Hu, M.; Goicochea, J. V.; Michel, B.; Poulikakos, D. *Appl. Phys.*
542 *Lett.* **2009**, 95 (15), 191503.
543 (55) Hu, M.; Wang, X.; Hartland, G. V.; Salgueirino-Maceira, V.;
544 Liz-Marzan, L. M. *Chem. Phys. Lett.* **2003**, 372 (5–6), 767–772.
545 (56) Pastoriza-Santos, I.; Perez-Juste, J.; Liz-Marzan, L. M. *Chem.*
546 *Mater.* **2006**, 18 (10), 2465–2467.
- (57) Gorelikov, I.; Matsuura, N. *Nano Lett.* **2008**, 8 (1), 369–373. 547
(58) Murphy, C. J.; San, T. K.; Gole, A. M.; Orendorff, C. J.; Gao, 548
J. X.; Gou, L.; Hunyadi, S. E.; Li, T. *J. Phys. Chem. B* **2005**, 109 (29), 549
13857–13870. 550
(59) Alpert, J.; Hamad-Schifferli, K. *Langmuir* **2010**, 26 (6), 3786– 551
3789. 552
(60) Shiotani, A.; Mori, T.; Niidome, T.; Niidome, Y.; Katayama, Y. 553
Langmuir **2007**, 23 (7), 4012–4018. 554